Heliyon 9 (2023) e18490

Contents lists available at ScienceDirect

Heliyon

journal homepage: www.cell.com/heliyon

Temozolomide and chloroquine co-loaded mesoporous silica nanoparticles are effective against glioma

Peng Zhang [a], Fang Cao [a], Jiqin Zhang [b], Ying Tan [c,*], Shengtao Yao [a,**]

[a] Department of Neurosurgery, Affiliated Hospital of Zunyi Medical University, Guizhou, 563000, PR China
[b] Department of Anesthesiology, Guizhou Provincial People's Hospital, Guizhou, 550002, PR China
[c] Department of Neurosurgery, Guizhou Provincial People's Hospital, Guizhou, 550002, PR China

ARTICLE INFO

Keywords:
Glioma
Mesoporous silica nanoparticles
Autophagy
Chloroquine
Apoptosis

ABSTRACT

The past decades have witnessed great progress in nanoparticle-based cancer-targeting drug delivery systems, but their therapeutic potentials is yet to be fully exploited. In this research, temozolomide (TMZ) and chloroquine (CQ) were loaded into the mesoporous silica nanoparticles (MSNs), the surface was coated with polydopamine (PDA), and the complex was coupled with arginine-glycine-aspartic (RGD) to successfully prepare TMZ/CQ@MSN-RGD. RGD-MSNs accumulated more in the cell and tumor models than in unmodified MSNs in the in vitro and in vivo experiments and can directly induce apoptosis and autophagy in tumor cells. In addition, TMZ/CQ@MSN-RGD therapy enhanced the apoptosis effect of the RGD-MSNs in glioma. Therefore, the combination of autophagy inhibitor with chemotherapy drugs in nanocarriers may promote therapeutic efficacy in treating glioma.

1. Introduction

Glioma is the most common tumor in the adult central nervous system, and its morbidity and mortality are increasing, Most patients are between 6 and 80 years old [1]. The DNA-alkylating agent, temozolomide (TMZ), is the most widely used and clinically recognized chemotherapeutic drug. However, many drugs including TMZ，have nosignificant anticancer efficacy because of their poor solubility, rapid clearance, side effects and resistance [2,3]. In addition, traditional anti-cancer drugs cannot target tumor tissue but accumulate inside normal tissues, causing side effects. Therefore, to prevent toxic effects, lower doses of drugs are often used, which may activate the autophagy-protective mechanism of tumor cells, lead to drug resistance and limit therapeutic efficacy. Therefore, highly efficient targeted drug delivery strategies are urgently needed in specific locations to improve the targeting of tumors, inhibit accumulation in non-tumor tissues, improve drug delivery, prevent the self-protection mechanism of cancer cells, and finally achieve effective treatment.

The emergence of nanotechnology has completely changed the process of drug delivery and targeted delivery, and it has even changed the precedent of the entire pharmaceutical industry [4,5]. Researchers have developed a variety of nanomedicines to improve drug delivery at specific sites and improve the safety and effectiveness of treatments. Mesoporous silica nanoparticles (MSNs) have

* Corresponding author. Guizhou Provincial People's Hospital, No.83 Zhongshan East Road, Nanming District, Guiyang City, Guizhou Province, 550002, PR China.
** Corresponding author. Affiliated Hospital of Zunyi Medical University, No.149 Dalian Road, Huichuan District, Zunyi City, Guizhou Province, 563000, PR China.
E-mail addresses: tanying@gz5055.com (Y. Tan), syzymu@foxmail.com (S. Yao).

https://doi.org/10.1016/j.heliyon.2023.e18490
Received 28 November 2022; Received in revised form 7 July 2023; Accepted 19 July 2023
Available online 20 July 2023

become increasingly important as promising drug carrier, because of their unique porous structures, which maintain good chemical stability, surface functionality, and biology [6,7].

The surfaces of MSNs cannot be directly modified because their surface reactive functional groups are not abundant. Polydopamine (PDA) is a dopamine derived synthetic melanin polymer that is simple to prepare and exhibits good biocompatibility and biosafety [8]. For the vast majority of drug carriers and ligands, PDA can be easily functionalized with a surface to have an anchoring point effect and further bind with ligand molecules [9]. Additionally, PDA is stable under alkaline conditions but decomposes under acidic conditions; these features can be exploited to achieve pH-responsive release in tumor tissues and intratumoral lysosomes [10,11].

The high expression of integrin αvβ3 in tumor cells or neovasculogenesis is extremely low in normal blood vessel tissues, and can be used as a target for tumor targeted therapy. Arginine-glycine-aspartic (RGD) can bind to integrin receptors, inhibit tumor migration and tumor neovasculogenesis, and improve the targeting of anti-tumor drugs [7]. Despite advances in nanotechnology, significant challenges remain. Cancer cells respond to adverse environmental stress primarily by producing a typical protective autophagy response. In the process of autophagy, tumor cells can encapsulate chemotherapeutic drugs into lysosomes to prevent drugs from interacting with target organelles, thereby reducing cytotoxicity and limiting antitumor effects [12]. The acidic environments of lysosomes can degrade foreign drugs and prevent cell damage [13]. In the process of autophagy, the autophagosome engulfs the nanoparticles and combines with the lysosome to form an autophagolysosome. Chloroquine (CQ), originally used in the treatment of malaria, has been proven to block autophagy by inhibiting the fusion of autophagosome and lysosome, and has been widely used in autophagy research [14–16]. CQ is safe when used in combination with anticancer drugs to block tumor-protective autophagy, enhance efficacy and exhibit acceptable toxicity. Therefore, nanocarriers loaded with chemotherapy drugs and autophagy inhibitors may be effective in targeting tumors. On the basis of the above analysis and reasons, TMZ and CQ were co-loaded into MSN, and new nanoparticles were prepared by connecting PDA and RGD to improve drug delivery efficiency and further improve the anti-tumor effect.

2. Materials and methods

2.1. Materials and cell lines

Mesoporous silica was purchased from Jiangsu Xianfeng nanomaterials technology Co., Ltd (Nanjing, China). Dopamine hydrochloride, temozolomide, polypeptide and chloroquine (CQ) were supplied by Bitai Biotechnology. (Shanghai, China). LysoTracker was purchased from Maokang Biological Technology Co., Ltd. (Shanghai, China). Rhodamine 6G (R105623) was purchased from Aladdin Reagent Co., Ltd. (Shanghai, China). U87 cell lines were purchased from the cell bank of Chinese Academy of Sciences (Shanghai, China). Rat cortical neuronal cells were purchased from Guangzhou Jennio Biotech Co., Ltd (Guangzhou, China). All antibodies were obtained from Cell Signal Technology (United States).

2.2. Material preparation and characterization

MSN (10 mg) was dispersed in a phosphate buffer solution (PBS) solution and mixed with CQ (10 mg/ml) and TMZ (10 mg/ml)/DMSO under magnetic agitation. Stirring was performed for more than 12 h. The supernatant was removed by highspeed centrifugation (12,000 rpm and 20 min) and washed to remove unloaded TMZ and CQ, and the obtained precipitate (TMZ/CQ@MSN) was then mixed with chlorinated dopamine in a ratio of 2:1 under vacuum. The mixture was dissolved in Tris-HCl buffer, and stirred for 24 h. The surface of MSN was covered by PDA. The PDA-coated TMZ/CQ@MSN and RGD were mixed with Tris buffer in a ratio of 4:1, stirred, centrifuged, washed, and dried in accordance with the preceding steps to produce TMZ/CQ@MSN-RGD. The drug standards were accurately weighed and used in preparing the standard solution, and the absorbance was measured at 254 and 330 nm with a uUV-2450 spectrophotometer to make the standard curve. The supernatant from the preceding steps was collected and combined with the standard curve for calculation to obtain the mass of the two drugs, drug loading rate (DL) = (mass of loaded drug/mass of MSNs) × 100%. MSN and TMZ/CQ@MSN-RGD were suspended in phosphate buffer (pH = 7.4) and their size, zeta potential and polydispersity index (PDI) were analyzed by a nanoparticle size analyzer (Zetasizer Nano ZS90, Malvern Instruments, Worcestershire, UK) at room temperature. Nicolet™ IS™ 10 Fourier transform infrared (FT-IR) spectrometer was used to analyze the characteristic functional groups before and after MSN modification. The samples were detected with a transmission electron microscope and photographed.

2.3. In vitro drug release

TMZ/CQ@MSN-RGD (1.0 mg) was dispersed and stirred in 10 ml of PBS (100 UG/ml), and different pH values (5.0, 6.5, and 7.4) were adjusted. The homogeneously dispersed suspension was centrifuged at different time periods, and the supernatant was collected for UV absorbance analysis (254 and 343 nm). The release amounts of the two drugs were calculated and averaged, and the release profiles were obtained by plotting the absorbance values of the released drugs against time.

2.4. In vitro cytotoxicity experiments

U87 cells were plated at a density of 1×10^4 cells per well and seeded in 96 well plates (three wells per group) and incubated in an incubator at 37 °C and 5% CO2 until 80% cell confluence was reached. Various concentrations of TMZ, TMZ@MSN-RGD, and TMZ/CQ@MSN-RGD were prepared for 24 h. A CCK-8 cell viability assay reagent was added for 2 h. The absorbance values (OD values) of

the samples at 450 nm were detected by a microplate reader. MSN and TMZ/CQ@MSN-RGD appropriate drug concentrations were selected to treat the rat cortical neuronal cells by the experiments described previously, and cell activity was calculated by detecting the absorbance values (OD values).

2.5. Cellular uptake and subcellular localization of NPs

U87 cells were cultured in DMEM medium with 10% fetal bovine serum and 1% penicillin-streptomycin at 37 °C and 5% CO_2 atmosphere. We synthesized R6G@MSN and R6G@TMZ-RGD by using rhodamine 6G (R6G) instead of TMZ and observed intracellular fluorescence at 530 nm excitation wavelength. R6G@MSN and R6G@MSN-RGD (R6G = 50 μg/ml) were cultured in different dishes of U87 cells at the logarithmic growth stage. The supernatant collected, and excess nanoparticles were washed with PBS. Inverted fluorescence microscopy (Nikon TE2000U, Japan) was used to detect the uptake of nanoparticles by the U87 cells. Lysotracker green with 50 nM (Thermo, l7526) was co cultured with cells for 3 h, and lysosomes were labeled with green fluorescence. The cells were washed three times with PBS, and cell culture was continued for 24 h in a medium containing R6G@MSN-RGD or R6G@MSN. The treatment concentration and method were the same as those described above. Fluorescence was then observed and imaged using a confocal microscope (Leica SP2, Heidelberg, Germany).

2.6. Autophagy and apoptosis analyses

U87 cells cultured at the logarithmic growth stage were treated with PBS, TMZ, TMZ@MSN-RGD, TMZ/CQ@MSN-RGD for 24 h (TMZ = 50 μg/ml, CQ = 50 μg/ml), and the proteins were extracted and determined by the BCA protein assay method. Western blotting (WB) was used to determine the effect of nanoparticles on the expression level of related proteins, including p62 (CST, #88588), LC3B(CST, #9664), caspase3 (CST, #3510) and GAPDH (CST, #2118). The target proteins were detected with chemiluminescence reagents with the Bio-Rad imaging system. U87 cells were collected in the same manner, and apoptosis was detected by flow cytometry.

2.7. Xenograft tumor model

A total of 24 healthy male nude mice were provided and raised by experimental Animal Center of Zunyi Medical University. All animal experiments were performed according to the strict rules of the National Institutes of Health Guide for the Care and Use of Laboratory animals (NIH Publications No. 8023, revised 1978), and approved by the ethics committee of Affiliated Hospital of Zunyi Medical University (approval number: KLL-2020-156). PBS solution (100 μl; 1×10^5) containing U87 cells was injected subcutaneously into 4-week-old male nude mice. Tumor formation was observed every 3 days according to the following formula: $V = 1/2\ AB^2$ and tumor volume was recorded.

2.6. Anticancer effect in vivo

Once tumors reached 100 mm^3, 24 tumor-bearing mice were randomly divided into four groups to evaluate the therapeutic effect: control (saline); TMZ (5 mg/kg); TMZ@MSN-RGD (TMZ = 5 mg/kg); and TMZ/CQ@MSN-RGD (TMZ = 5 mg/kg) treatment groups. The drug was injected intraperitoneally every 2 days. After 33 days of treatment, all mice were anesthetized and by neck removal. The tumor was completely resected, measured and weighed, and made into paraffin sections. The level of apoptosis in tumor tissues was measured using a TUNEL Cell Death Detection Kit (Roche Molecular Biochemicals, Germany).

2.7. Nanosystem safety assessment

Ten 4-week-old healthy nude mice were randomly divided into experimental group and control group. TMZ/CQ@MSN-RGD at a concentration of 120 mg/kg was intraperitoneally injected into healthy nude mice, and saline was used as a control every 3 days for 1 month. During the experiment, the psychological state, diet and body weights of the nude mice were monitored. After 1month the mice were anesthetized and sacrificed by cervical vertebra dislocation. The main organs were removed and fixed with 4% paraformaldehyde for paraffin sectioning. After HE staining, they were observed under the microscope.

2.8. Statistical analysis

Each group had at least three replicates and the results were averaged. SPSS 22.0 software was used for statistical analysis. Comparison between groups was performed by one-way ANOVA and LSD-T test. $P < 0.05$ was considered statistically significant.

3. Results

3.1. Characterization of NPs

The specific surface area of MSN was 765.7 m^2/g, and the average pore size was 5–7 nm according to the technical parameters provided by the company. MSNs and TMZ@MSN-RGD had aqueous hydrodynamic diameters of 191.7 and 197.3 nm and

have good solubility in physiological solutions (Fig. 1A). The PDI of the MSNs was 0.342, whereas that of TMZ@MSN-RGD was 0.370. The zeta potential of MSNs and TMZ/CQ@MSN-RGD dispersed in water were −1.51 ± 6.22 and 38.8 ± 7.33 mV, respectively (Fig. 1B). Differences in particle size and FTIR spectra between TMZ/CQ@MSN-RGD and MSNs confirmed the successful combination of PDA and RGD with MSN (Fig. 1C). TMZ/CQ@MSN-RGD detected characteristic peaks at 3600 and 2000 - 1500 cm^{-1} by an infrared spectrometer, which directly confirmed the connection between PDA and RGD. TEM examination of MSNs and TMZ/CQ@MSN-RGD samples revealed that the two kinds of nanoparticles were uniform spherical structures, and our processing and modification did not change the shapes of the material surfaces. In addition, the materials were well dispersed and the mesoporous channels were closely distributed on the surfaces of the MSNs. (Fig. 1D). **The drug loading efficiency rates of TMZ and CQ were 8.5% and 7.6%, respectively, which were** calculated spectrophotometrically at 254 and 330 nm.

3.2. *In vitro drug release and cytotoxicity*

The cytotoxicity of various TMZ formulations against U87 cells was concentration dependent, and the IC50 values after TMZ, TMZ@MSN-RGD, and TMZ/CQ@MSN-RGD treatment for 24 h were 24.48, 104.3, and 61.08 μg/ml, respectively (Figure S1). To demonstrate the biosafety of the nanoparticles, we incubated rat cortical neuronal cells at an MSN concentration of 1000 μg/ml for 72 h, and the resulting cell viability was still greater than 80% (Figure S2). We examined the drug release in vitro at pH 5.0, pH 6.5, and pH 7.4. Approximately 55.97% of the drug was released from the nanoparticles in the pH 7.4 buffer; 76.47% of the drug was released from the nanoparticles in the pH 6.5 buffer; and 96.61% of the drug was released from the nanoparticles in the pH 5.0 buffer. Additionally, the amount of drug release was time-dependent under different pH conditions (Fig. 1E). Cellular uptake and subcellular localization of nanoparticles.

As shown in Fig. 2A, under an inverted fluorescence microscope, the uptake of MSNs modified with RGD by cells was significantly higher than that of the non-RGD group, and statistically significant difference was found (P = 0.0315). When the co-culture time of R6G@MSN-RGD and cells was extended to 24 h, the uptake rate of nanoparticles was increased, and the difference was statistically significant (P = 0.0305). The lysosome was labeled with lysotracker with green fluorescence. We found that when R6G@MSN was modified by RGD, the intensity of red fluorescence in cells representing nanoparticles increased, and a large number of nanoparticles were located in the lysosomes. The red fluorescence overlapped with the green fluorescence, and intense yellow fluorescence was

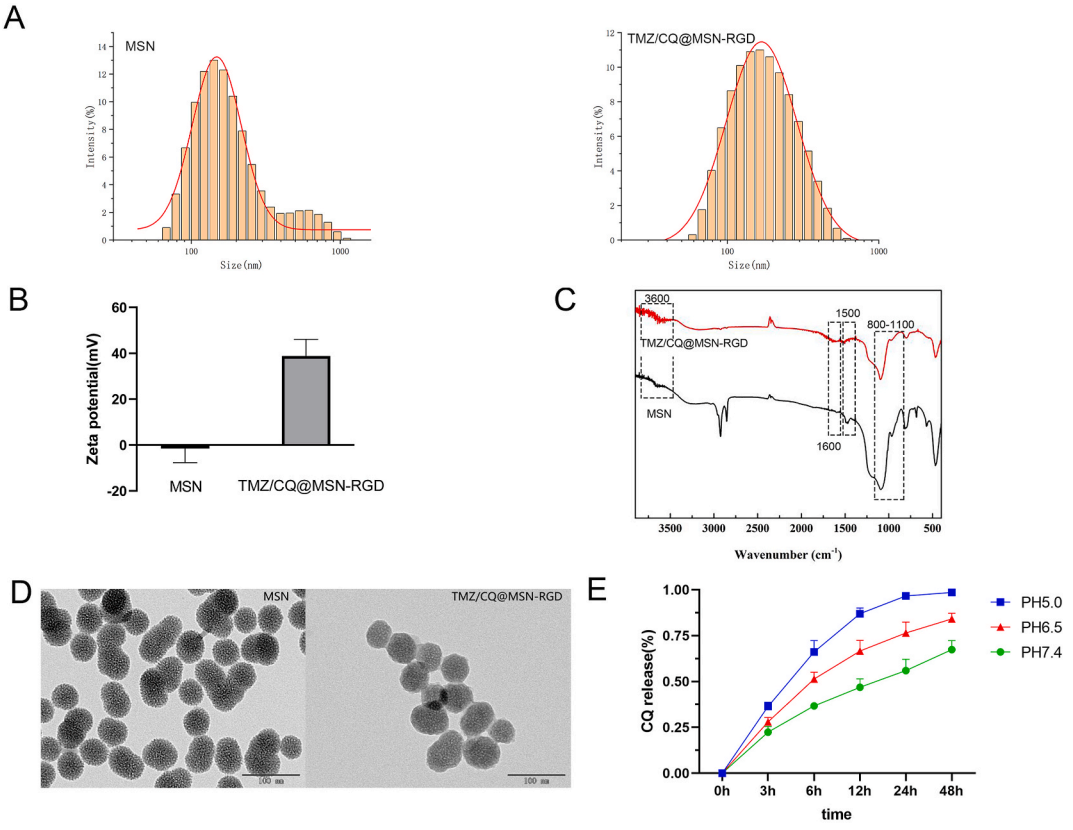

Fig. 1. A, The size of MSNs and TMZ/CQ@MSN-RGD detected by Zetasizer Nano ZS90. B, The zeta potential of MSNs and TMZ/CQ@MSN-RGD detected by Zetasizer Nano ZS90. C, FTIR spectrum of MSNs and TMZ/CQ@MSN-RGD. D,TEM examination of MSNs and TMZ@MSN-RGD. Scale bar: 100 nm. E, In vitro releasement of TMZ/CQ@MSN-RGD

observed under the confocal microscopy (Fig. 2B).

3.3. Autophagy and apoptosis analysis

Through WB, we found that the same amount of TMZ@MSN-RGD induced higher levels of autophagy and apoptosis than TMZ alone, p62 level was reduced, and LC3BIIand caspase3 levels were increased. In the CQ co-loading group, autophagy and p62 degradation was inhibited, whereas the expression level of the apoptotic protein caspase3 further increased (Fig. 3A). Cell apoptosis in each group was detected by flow cytometry (Fig. 3B). TMZ treatment induced apoptosis in 20.41% of U87 cells, whereas TMZ@MSN-RGD induced apoptosis in 38.24%. Moreover, apoptosis was detected in 58.26% of cells in the CQ co-loading group. The above results indicated that the same amount of TMZ@MSN-RGD can induce the autophagy and apoptosis of U87 cells to higher degree than TMZ alone. The autophagy of tumor cells was inhibited and apoptosis was significantly increased when the autophagy inhibitor CQ was used.

3.4. Antitumor efficacy of TMZ/CQ@MSN-RGD *in vivo*

Twenty-four male mice were successfully established as tumor models. Compared with the TMZ group, the TMZ@MSN-RGD group had a slower tumor growth rate, and the tumor volume was smaller after the nude mice were sacrificed. In the four groups, the combination of TMZ/CQ@MSN-RGD had the best inhibitory effect on tumor growth rate and volume (Fig. 4A and B). TUNEL staining

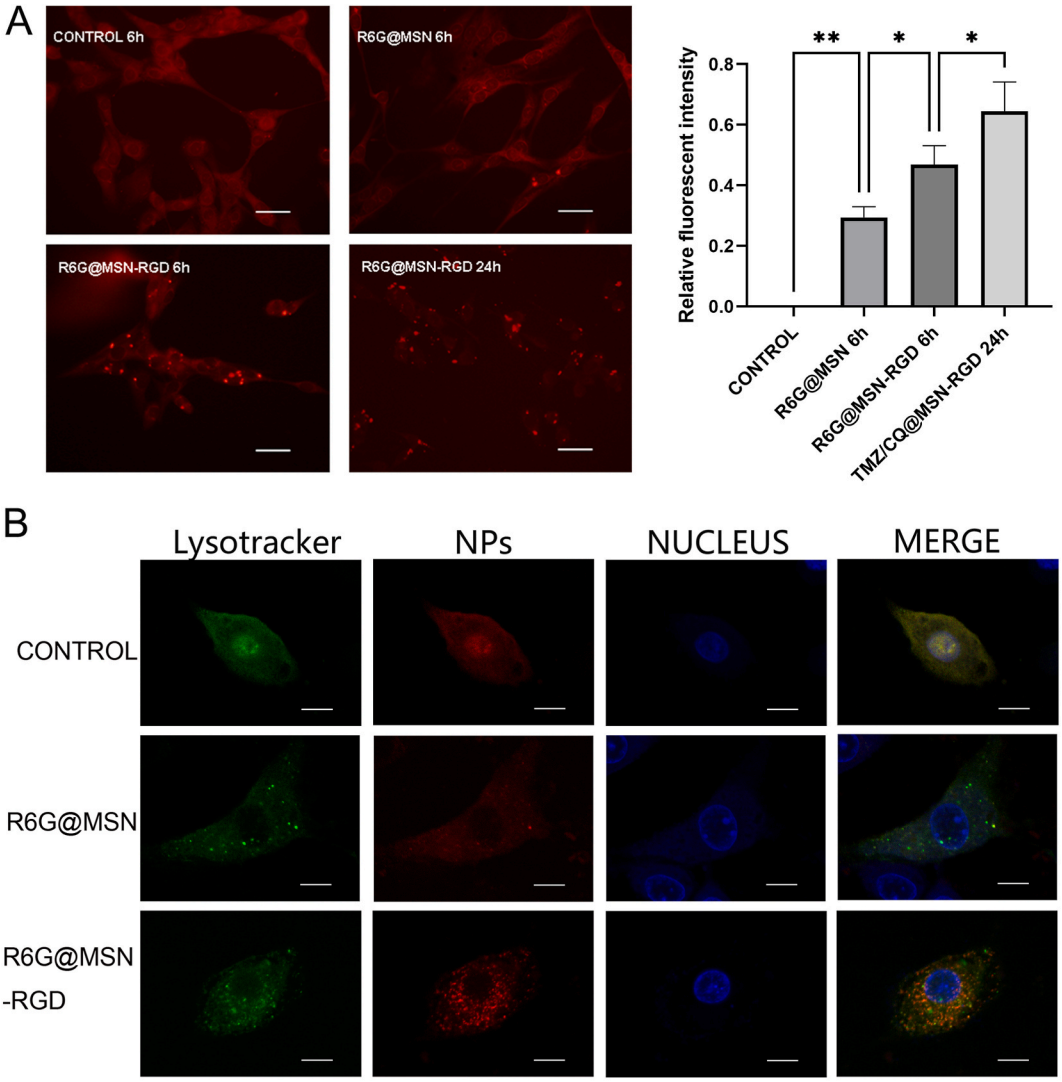

Fig. 2. A, Cell uptake of different nanoparticles at different time periods. Scale bar: 100 μm. B, Localization of nanoparticles and lysosome. Scale bar: 10 μm .

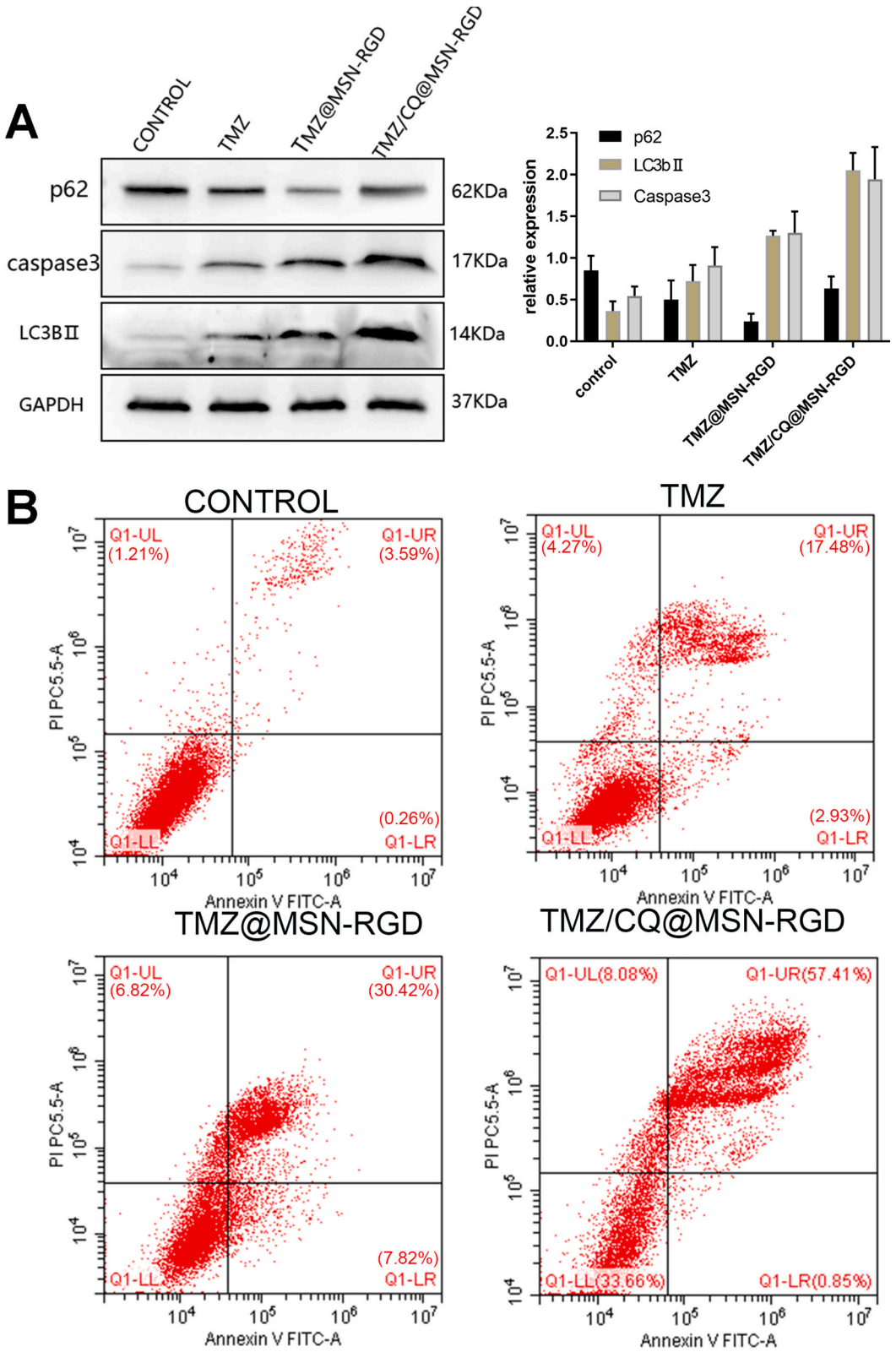

Fig. 3. A, The expression of p62, LC3B and caspase3 in U87 cells after different treatments. B, The apoptosis of U87 cells detected by flow cytometry after different treatments.

of tumor tissue sections showed that the number of TUNEL-positive cells (green spots) increased in the TMZ@MSN group, and few green spots were observed in the TMZ group, which was statistically significant at P = 0.00499. Compared with the TMZ@MSN-RGD group, the number of TUNEL positive cells in the TMZ/CQ@MSN-RGD group significantly increased (Fig. 5), and difference was statistically significant at P = 0.0056. In addition, the HE staining of major organs and body weight monitoring confirmed that the

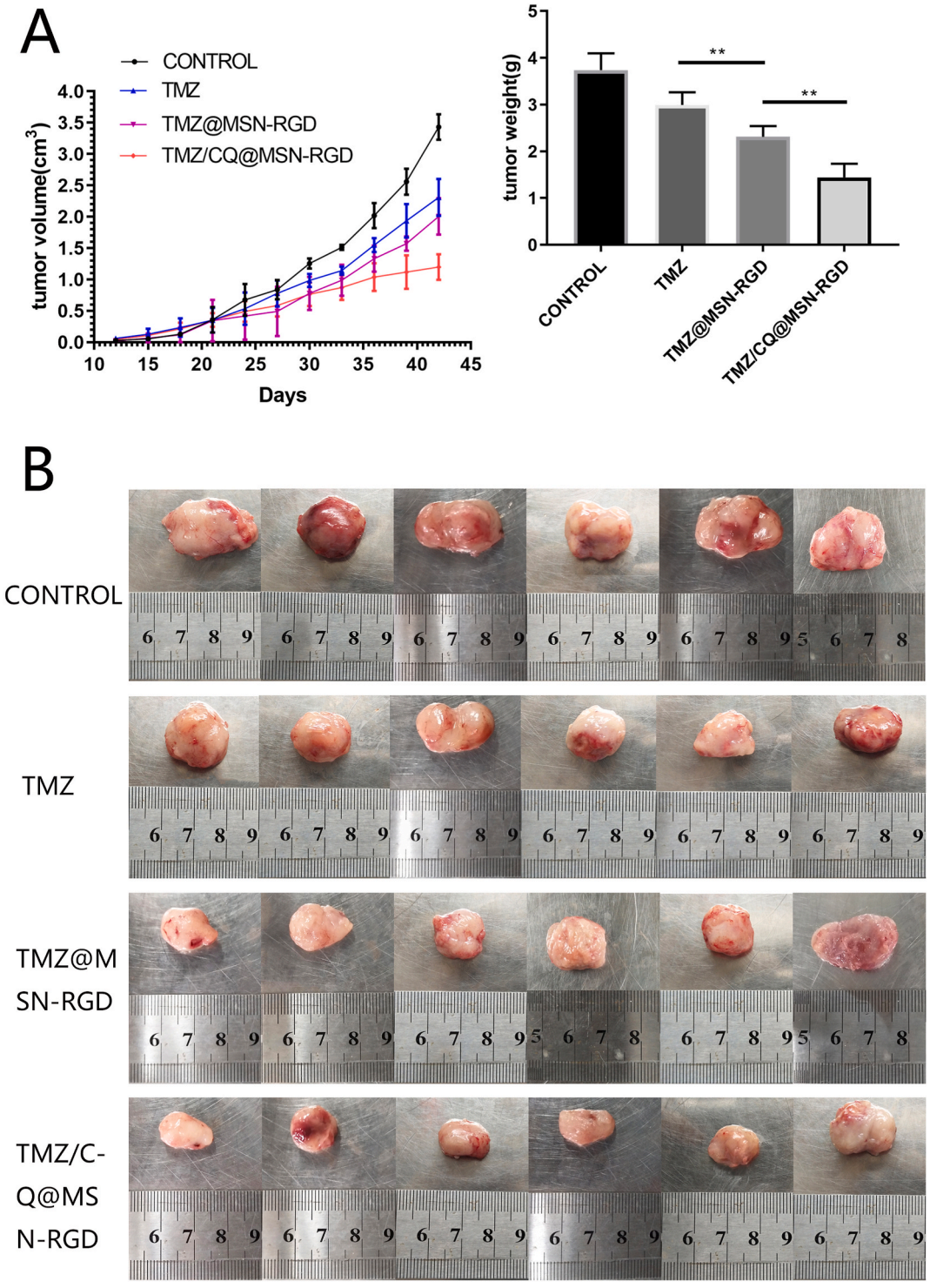

Fig. 4. A, Tumor volume and weight of the U87 xenografts. B, Xenografts from the control, TMZ, TMZ@MSN-RGD, and TMZ/CQ@MSN-RGD groups.

nanodrug-loading system was not significantly toxic (Figure S3).

4. Discussion

Glioma is the most common malignant brain tumor, accounting for about 80% of brain tumors. Chemotherapy drugs are subject to drug dosage, drug toxicity, chemotherapy resistance and other factors, which seriously affect the prognosis. In this study, TMZ and CQ were loaded into MSNs, and the polypeptide RGD was used to increase the targeting ability. The drug-loaded nanoparticle exhibited of targeted therapy, had low toxic potency, reduced chemotherapy resistance, and inhibited the proliferation of glioma cells.

To reduce the drug dosage and the toxicity of chemotherapy drugs and improve targeting, nanomaterials have be used in the field of cancer treatment. We selected mesoporous silica as nanocarriers to prepare MSNs with a particle size of about 90 nm. Nanoparticles with a smaller particle size are more likely to be taken up by cells, and easily cross the blood-brain barrier. MSN mesopores were loaded with TMZ and CQ in optimal mass ratios, and PDA was coupled with RGD, which can specifically bind to integrins on tumor cells, promote neovascularization, and increase nanoparticle uptake [17–19]. Changes in hydrated particle size and nanoparticle charge indirectly confirmed the relationship among drug loading, PDA, and RGD. In addition, FT-IR analysis determined the surface modification of MSNs. The pristine MSN showed peaks between 1100 and 800 cm^{-1}, which corresponded to the Si–O and Si–O–Si vibrations of silanol groups and different bonds and hydroxyl groups on the surfaces of the MSNs. The characteristic peak around 1600 cm^{-1} was attributed to the C═C bond stretching vibration of PDA. The stretching vibration of N–H at 3600 cm^{-1} and the ~1500 cm^{-1} amide characteristic peaks proved the formation of amide bonds between PDA and RGD. These results, identical to those of similar studies, demonstrated the successful modification of PDA and RGD on the surfaces of MSNs [20,21].

However, owing to the toxicity of TMZ and the chemoresistance of tumors, improving its therapeutic efficacy is still an urgent goal. Taking advantage of the unstable property of PDA under acidic conditions, we endowed the nanodrug loaded system with pH dependence. Specifically, this nanoparticle was stable under neutral conditions, and it released the drug easily under acidic conditions. This characteristic is favorable for its release in the acidic microenvironments of tumors, especially in lysosomes (pH = 5) inside tumor cells, which can enhance the targeting of drugs and inhibit the targeting of normal cells. In addition, autophagy plays a role in tumor survival and death. Most studies believe that autophagy plays a positive role in glioma survival, helping tumor cells survive in harsh environments. TMZ induces survival autophagy through the ATM/AMPK/ULK1 and RTK/Ras/PI3K pathways, thereby promoting glioma chemotherapy resistance [22–24]. Enhanced survival autophagy further complicates glioma pathogenesis and response to therapy. However, CQ can destroy the stability of lysosomes and activate P53, affecting the formation of autophagy lysosomes, thereby reducing the protective effect of autophagy and resulting in a higher level of apoptosis of glioma cells [25,26]. These effects were reflected in the WB experiment in TMZ/CQ@MSN-RGD group, the expression of autophagy-related proteins decreased, and the expression of apoptotic proteins increased. The apoptosis rate of the TMZ/CQ@MSN-RGD group significantly increased. In addition, some studies believe that the uptake of lysosomes is one of the main factors affecting the efficiency of plasmids or transfection, and the destruction of lysosomes by CQ can significantly improve the drug delivery efficiency of nanomaterials and increase the efficiency of chemical drugs [27,28]. In the present study, WB, flow cytometry and other experiments confirmed that TMZ@MSN-RGD can induce autophagy and apoptosis, and TMZ/CQ@MSN-RGD combined with CQ can inhibit autophagy, block its protective effect, and induce intense apoptosis. In the animal experiments, the TMZ/CQ@MSN-RGD group had the strongest anti-tumor effect and the smallest tumor growth rate and final volume. In addition, TUNEL staining showed that the TMZ/CQ@MSN-RGD group led to a higher level of apoptosis. The combination of nanodrug delivery systems and autophagy inhibitors represent a novel direction for cancer therapy, but larger sample sizes and deeper mechanistic studies are needed to evaluate their effectiveness.

Author contribution statement

Peng Zhang; Ying Tan; Shengtao Yao: Conceived and designed the experiments; Performed the experiments; Analyzed and interpreted the data; Contributed reagents, materials, analysis tools or data; Wrote the paper.

Fang Cao; Jiqin Zhang: Conceived and designed the experiments; Analyzed and interpreted the data; Wrote the paper.

Funding statement

This work was supported by Guizhou Provincial Science and Technology Projects ([2020]1Z066 and QKHJC-ZK[2021]YB473), Zunyi Science and Technology Projects (ZSKHHZZ[2020]254).

Data availability statement

Data will be made available on request.

Declaration of competing interest

The authors declare that they have no known competing financial interests or personal relationships that could have appeared to influence the work reported in this paper.

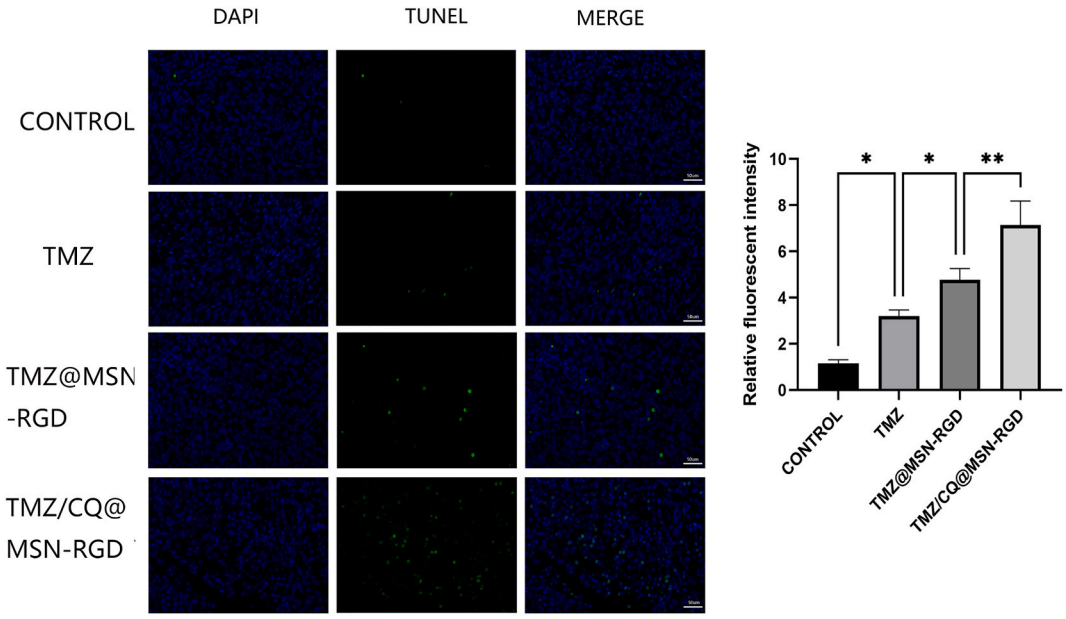

Fig. 5. Fluorescence microscope images of TUNEL staining after different treatments. Scale bar: 100 μm.

Appendix A. Supplementary data

Supplementary data related to this article can be found at https://doi.org/10.1016/j.heliyon.2023.e18490.

References

[1] S. Lapointe, A. Perry, N.A. Butowski, Primary brain tumours in adults, Lancet (London, England) 392 (10145) (2018) 432–446.
[2] W. Wu, J.L. Klockow, M. Zhang, F. Lafortune, E. Chang, L. Jin, Y. Wu, H.E. Daldrup-Link, Glioblastoma multiforme (GBM): an overview of current therapies and mechanisms of resistance, Pharmacol. Res. 171 (2021), 105780.
[3] M.A. Dymova, E.V. Kuligina, V.A. Richter, Molecular mechanisms of drug resistance in glioblastoma, Int. J. Mol. Sci. 22 (12) (2021).
[4] S. Cheng, S.K. Nethi, S. Rathi, B. Layek, S. Prabha, Engineered mesenchymal stem cells for targeting solid tumors: therapeutic potential beyond regenerative therapy, J. Pharmacol. Exp. Therapeut. 370 (2) (2019) 231–241.
[5] M. Ovais, S. Mukherjee, A. Pramanik, D. Das, A. Mukherjee, A. Raza, C. Chen, Designing stimuli-responsive upconversion nanoparticles that exploit the tumor microenvironment, Advanced materials (Deerfield Beach, Fla) 32 (22) (2020), e2000055.
[6] Y. Alyassin, E.G. Sayed, P. Mehta, K. Ruparelia, M.S. Arshad, M. Rasekh, J. Shepherd, I. Kucuk, P.B. Wilson, N. Singh, et al., Application of mesoporous silica nanoparticles as drug delivery carriers for chemotherapeutic agents, Drug Discov. Today 25 (8) (2020) 1513–1520.
[7] R.K. Kankala, Y.H. Han, H.Y. Xia, S.B. Wang, A.Z. Chen, Nanoarchitectured prototypes of mesoporous silica nanoparticles for innovative biomedical applications, J. Nanobiotechnol. 20 (1) (2022) 126.
[8] I.S. Kwon, C.J. Bettinger, Polydopamine nanostructures as biomaterials for medical applications, J. Mater. Chem. B 6 (43) (2018) 6895–6903.
[9] J. Hu, Q. Wang, Y. Wang, G. You, P. Li, L. Zhao, H. Zhou, Polydopamine-based surface modification of hemoglobin particles for stability enhancement of oxygen carriers, J. Colloid Interface Sci. 571 (2020) 326–336.
[10] H. Wu, M. Wei, Y. Xu, Y. Li, X. Zhai, P. Su, Q. Ma, H. Zhang, PDA-based drug delivery nanosystems: a potential approach for glioma treatment, Int. J. Nanomed. 17 (2022) 3751–3775.
[11] C. Zhou, Q. Yang, X. Zhou, N. Jia, PDA-coated CPT@MIL-53(Fe)-based theranostic nanoplatform for pH-responsive and MRI-guided chemotherapy, J. Mater. Chem. B 10 (11) (2022) 1821–1832.
[12] Y. He, B. Kaina, Are there thresholds in glioblastoma cell Death responses triggered by temozolomide? Int. J. Mol. Sci. 20 (7) (2019).
[13] N.A. Hussein, S. Malla, M.A. Pasternak, D. Terrero, N.G. Brown, C.R. Ashby Jr., Y.G. Assaraf, Z.S. Chen, A.K. Tiwari, The role of endolysosomal trafficking in anticancer drug resistance, Drug Resist. Updates : reviews and commentaries in antimicrobial and anticancer chemotherapy 57 (2021), 100769.
[14] M. Mauthe, I. Orhon, C. Rocchi, X. Zhou, M. Luhr, K.J. Hijlkema, R.P. Coppes, N. Engedal, M. Mari, F. Reggiori, Chloroquine inhibits autophagic flux by decreasing autophagosome-lysosome fusion, Autophagy 14 (8) (2018) 1435–1455.
[15] J. Beauvarlet, R. Nath Das, K. Alvarez-Valadez, I. Martins, A. Muller, E. Darbo, E. Richard, P. Soubeyran, G. Kroemer, J. Guillon, et al., Triarylpyridine compounds and chloroquine act in concert to trigger lysosomal membrane permeabilization and cell Death in cancer cells, Cancers 12 (6) (2020).
[16] J. Peng, Q. Wang, J. Zhou, S. Zhao, P. Di, Y. Chen, L. Tao, Q. Du, X. Shen, Y. Chen, Targeted lipid nanoparticles encapsulating dihydroartemisinin and chloroquine phosphate for suppressing the proliferation and liver metastasis of colorectal cancer, Front. Pharmacol. 12 (2021), 720777.
[17] H. Cui, L. Zhang, S. Zeng, Y. Wang, Z. Li, J. Wang, Q. Chen, Charge-reversible pro-ribonuclease enveloped in virus-like synthetic nanocapsules for systemic treatment of intractable glioma, ACS Appl. Mater. Interfaces 14 (27) (2022) 30493–30506.
[18] R.S. Garcia Ribeiro, S. Belderbos, P. Danhier, J. Gallo, B.B. Manshian, B. Gallez, M. Bañobre, M. de Cuyper, S.J. Soenen, W. Gsell, et al., Targeting tumor cells and neovascularization using RGD-functionalized magnetoliposomes, Int. J. Nanomed. 14 (2019) 5911–5924.
[19] H. Gao, C. Chu, Y. Cheng, Y. Zhang, X. Pang, D. Li, X. Wang, E. Ren, F. Xie, Y. Bai, et al., In situ formation of nanotheranostics to overcome the blood-brain barrier and enhance treatment of orthotopic glioma, ACS Appl. Mater. Interfaces 12 (24) (2020) 26880–26892.
[20] D. Fang, T. Li, Z. Wu, Q. Wang, M. Wan, M. Zhou, C. Mao, Dual drive mode polydopamine nanomotors for continuous treatment of an inferior vena cava thrombus, J. Mater. Chem. B 9 (41) (2021) 8659–8666.

[21] L. Chen, B. Wang, H. Ren, Y. Wu, D. Lyu, Y. Ouyang, Q. Zhang, Y. Yan, Arg-Gly-Asp peptide functionalized poly-amino acid/poly (p-benzamide) copolymer with enhanced mechanical properties and osteogenicity, Biomater Adv 133 (2022), 112627.
[22] Y. Zou, Q. Wang, B. Li, B. Xie, W. Wang, Temozolomide induces autophagy via ATM-AMPK-ULK1 pathways in glioma, Mol. Med. Rep. 10 (1) (2014) 411–416.
[23] B.G. Harder, S. Peng, C.P. Sereduk, A.M. Sodoma, G.J. Kitange, J.C. Loftus, J.N. Sarkaria, N.L. Tran, Inhibition of phosphatidylinositol 3-kinase by PX-866 suppresses temozolomide-induced autophagy and promotes apoptosis in glioblastoma cells, Mol. Med. (Camb.) 25 (1) (2019) 49.
[24] F. Tang, C. Yang, F.P. Li, D.H. Yu, Z.Y. Pan, Z.F. Wang, Z.Q. Li, Palmitoyl transferases act as potential regulators of tumor-infiltrating immune cells and glioma progression, Mol. Ther. Nucleic Acids 28 (2022) 716–731.
[25] J. Pelt, S. Busatto, M. Ferrari, E.A. Thompson, K. Mody, J. Wolfram, Chloroquine and nanoparticle drug delivery: a promising combination, Pharmacol. Therapeut. 191 (2018) 43–49.
[26] Y.S. Hori, R. Hosoda, Y. Akiyama, R. Sebori, M. Wanibuchi, T. Mikami, T. Sugino, K. Suzuki, M. Maruyama, M. Tsukamoto, et al., Chloroquine potentiates temozolomide cytotoxicity by inhibiting mitochondrial autophagy in glioma cells, Journal of neuro-oncology 122 (1) (2015) 11–20.
[27] M. Brueckner, K. Scheffler, U. Reibetanz, Enhanced cytoplasmic release of drug delivery systems: chloroquine as a multilayer and template constituent of layer-by-layer microcarriers, J. Mater. Chem. B 6 (31) (2018) 5153–5163.
[28] M. Hajimolaali, H. Mohammadian, A. Torabi, A. Shirini, M. Khalife Shal, H. Barazandeh Nezhad, S. Iranpour, R. Baradaran Eftekhari, F. Dorkoosh, Application of chloroquine as an endosomal escape enhancing agent: new frontiers for an old drug, Expet Opin. Drug Deliv. 18 (7) (2021) 877–889.